Int. J. Electrochem. Sci., 16 **(2021)** Article ID: 210541, doi: 10.20964/2021.05.08

International Journal of
ELECTROCHEMICAL
SCIENCE
www.electrochemsci.org

Synthesis of Graphene/$Ni(OH)_2$ Composite with Excellent Pseudocapacitive Performance

Zhixin Ge[1], Yu-qiu Huo[2], Dewen Zheng[1], Qian Zhang[1]*

[1] Research Institute of Petroleum Exploration and Development- Langfang, China, 6500
[2] Department of Chemistry, College of Science, Northeastern University, Shenyang, China, 110819
[*]E-mail: huoyuqiu@mail.neu.edu.cn

Received: 30 December 2020 / *Accepted:* 1 March 2021 / *Published:* 31 March 2021

Sandwich structure graphene/$Ni(OH)_2$ composites with super pseudocapacitive performance are obtained by one-pot hydrothermal method. Thermogravimetry and differential scanning calorimetry (TG–DSC), X-ray diffraction (XRD) analysis, Scanning electron microscopy (SEM), Fourier transformed infrared spectroscopy (FTIR), Raman spectroscopy (Ram) and Transmission electron microscopy (TEM) are used to determine the structure and morphology of the composites. It is interesting that the C : Ni ratio plays an important role on the composite's capacitive performance. The specific capacitance is 2256 F g^{-1} at 6M KOH solution when the ratio of C:Ni is 1:7. 93% specific capacitance is remained after 7000 cycles, which exhibits its superior cycle stability. This reflects that sandwich structure graphene/$Ni(OH)_2$ materials are promising for energy storage applications.

Keywords: Graphene; $Ni(OH)_2$; Sandwich structure; Capacitance performance

1. INTRODUCTION

Supercapacitors, combined high energy densities and excellent power density, paving a way between traditional batteries and conventional electric double-layer capacitors (EDLC) [1, 2]. Beyond this, supercapacitors possess high rate capability and long recycling life. They are promising in portable electronic devices, power backup, and industrial energy management, etc [3, 4]. The unique characteristics of supercapacitors are relyed upon the fast and reversible redox reactions of active materials which is named pseudocapacitance[5, 6]. Actually, EDLC and the pseudocapacitance are both exist in the supercapacitors. But the pseudocapacitance is several dozens times of EDLC in most situations. This fast and reversible redox reaction can occur not only on the surface but also in the body of electrode, but primarily on the surfaces or near-surface areas of active materials especially under fast charging and discharging conditions. So an effective way to enhance energy density is to enlarge the surface area of active materials. Mainly there are two ways to realize this [7, 8]. First method,

which has been widely reported, is to control the morphology of materials, such as nanosized or porous structures. Another simple way is to synthesis super performance mixture or compounds. $Ni(OH)_2$ is a attractive supercapacitor materials because of its low price, environmental safety, facile synthesis and super theoretical specific capacitance (3750 F g^{-1}) [9,10]. But its poor conductivity (~10^{-17} S/cm) and volume changing during charging and discharging process prevents its directly application. A practicable method is to combine it with well conductive materials [11,12]. Graphene has attracted much attention since it was first obtained in 2004 by micromechanical cleavage method [13]. Graphene is a single-atom-thick of graphite structure. It possesses the advantages of both excellent conductivity and large surface area (2630m^2/g) [14-16]. Recently, graphene has gained great attention on enhancement the performance of supercapacitors [17, 18]. However, due to van der Waals interaction, graphene sheets usually agglomerate and loss its special performance during process of preparation. As a result, as well as we known, limited improvement has been gained until now (120−348 F g^{-1}) [19, 20]. The combination of $Ni(OH)_2$ with graphene prevent the agglomeration of graphene as well as improve the conductivity of $Ni(OH)_2$ and enlarge the effective surface area of electrode [21-23]. So the capacitive performance of graphene/$Ni(OH)_2$ is heavily enhanced. In this paper the $Ni(OH)_2$ nanosheets are in suit induced on the graphene surface through simple one-step hydrothermal method, and sandwich layered structure composites are obtained. In 6 M KOH solution, the maximum specific capacitance is 2256 F g^{-1} at 12.5 A g^{-1}. This is a promising method to massively produce graphene/$Ni(OH)_2$ with excellent capacitive performance.

2. EXPERIMENTAL

2.1 Preparation of Graphene oxide (GO)

GO is synthesized by an improved Hummer's method derived from graphite powder of reagent grade [24]. 2.0 g graphite powder together with 50 ml 98% H_2SO_4 solution were put into 0-10 ℃ ice bath and stirred for 30 minutes. Then 0.3 g $KMnO_4$ was added to preoxide 5 minutes while being vigorously stirred. After that 2 g $KMnO_4$ is gradually added for 3 times in turn within 20 ℃ under the same agitation condition. The compound is stirred at about 35 ℃ for 3 h. Further, 100 ml deionized water is bit by bit added to the admixture under vigorous agitation to keep temperature remain at about 90 to 100 ℃. In the end, 300 ml 50 ℃ deionized water and 30 ml 30% H_2O_2 are added under stirring within 15 minutes. The as-prepared products are filtered and in turn washed with 1% HCl solution to remove metal ions, and repeatedly washed with deionized water. The filter GO cake is dried in an 80 ℃ vacuum oven for 12 h.

2.2 Preparation of graphene/$Ni(OH)_2$

The 20mg GO was added into a certain quantity of nickel acetate $Ni(C_2H_3O_2)_2$ aqueous solution. Stirring 2 h before the admixture was sealed in a reacting still, and then put it into 200 °C oven to react 10h. The obtained was washed by deionized water and ethanol in turn for several times, before dried in an 80°C vacuum oven for 12 h. According to the ratio of C to Ni (1:1, 1:4, 1:7, 1:9,

1:13), the products are marked as G1, G2, G3, G4 and G5, respectively. For comparison, $Ni(OH)_2$ and graphene (GE) samples are also prepared in the same condition but without the presence of GO or $Ni(C_2H_3O_2)_2$.

2.3 Characterization and Electrochemical Test

The morphologies of the samples are examined with a scanning electron microscope (SEM, SU8010). The sample structure and chemical compositions are determined by X-ray diffraction (XRD, D8 ADVANCE) with Cu K_α (0.15416nm) source and energy dispersive X-ray spectroscope (EDX). Fourier transform infrared (FTIR) spectra are obtained by using VERTEX70. The thermal stable of samples structure are examined by thermogravimetry and differential scanning calorimetry (TG–DSC) on TGA/DSC1, the sweeping temperature range is 25-750 °C with a scanning step of 10 °C min^{-1} at argon atmosphere. The electrochemical behaviors of samples are determined by CHI660D. Cyclic voltammograms and galvanostatic charge–discharge tests are carried out within a three-electrode system. $Ni(OH)_2$, graphene or graphene/$Ni(OH)_2$ is used as the working electrode, platinum sheet is used as the counter electrode, and SCE is used as the reference electrodes, respectively.

3. RESULTS AND DISCUSSION

3.1 Structural characteristic

TG-DSC is conducted at argon to recognize the thermal stability of samples. As can be seen from Fig.1 (A), there is a gently slope before 100°C for $Ni(OH)_2$, it owning to the vaporization of moisture. Between 275 and 320 °C, the weight loss of about 16% along with a DSC exothermal peak, which owing to the following reaction (1):

$$Ni(OH)_2 \rightarrow NiO + H_2O \qquad (1)$$

In Fig. 1 (B), a rapid mass loss of about 13% from 250 to 310°C due to the same reaction (1) is detected in the graphene/$Ni(OH)_2$ (G3) sample. The decrease of the decomposition temperature indicates that the doped $Ni(OH)_2$ in the graphene/$Ni(OH)_2$ is more easily to be disintegrated than the pure $Ni(OH)_2$ sheet due to the aggregates of $Ni(OH)_2$ plate structures are dispersed by the intercalated graphene. The active sites of $Ni(OH)_2$ are enriched which resulting in the enhancement of its capacitive performance. The fractional variation of 3% is due to the contribution of graphene in the composite. The weight loss of about 15% between 650 and 750°C in Fig.1 (B) is owing to the oxidation of graphene by the water vapor produced by $Ni(OH)_2$ decomposion, which is shown in following Eqs. (2) and (3).

$$C+H_2O \rightarrow CO + H_2 \qquad (2)$$

$$C+2H_2O \rightarrow CO_2 + 2H_2 \qquad (3)$$

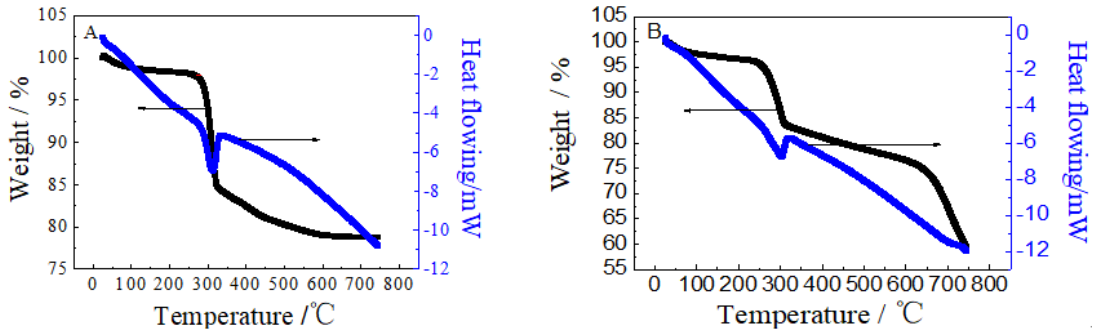

Figure 1. TG-DSC of $Ni(OH)_2$ (A) and graphene/$Ni(OH)_2$ (G3, B)

The natures of composites are further confirmed by XRD detection. XRD patterns of the graphene and G3 are given in Fig. 2A.The peak of graphene appears at 10.3°, which is its characteristic peak. The shift of 24° to 10.3° means the interlayer distances of the graphene is larger than that of graphite. It elucidates that graphene we prepared has more space for the ion and proton to transfer, which is benefit to the enhancement of conductivity and capacitive performance. The nearly symmetry of the (002) peak discloses the uniform interlayer spacing in c-axis direction. The diffraction peaks of the G3, at around 19.3°(001), 33.1°(100), 38.5°(101), 52.1°(102), 59.1°(110), 62.7°(111), 70.5°(103), 72.7°(201) and 82.6°(202), are those of hexagonal β-$Ni(OH)_2$ (JCPDS 14-0117). All the peaks, including 001, 100, 101, 102, 110, 111, 103, 201 and 202, are slim and relatively strong, which means the hexagonal β-$Ni(OH)_2$ crystallizes quite well. The characteristic peak of graphene is nearly disappeared in XRD patterns of G3, which is probably due to the degree of crystallinity of graphene is quite low compared with the β-$Ni(OH)_2$ crystal.

The presence of graphene and $Ni(OH)_2$ in the composites is further confirmed by FTIR spectroscopy. The benzene ring skeleton C=C stretching vibration peaks both appear at 1590 cm^{-1} for graphene /$Ni(OH)_2$ (G3) and graphene in Fig. 2(B). The new absorption peak at about 525 cm^{-1} in G3 is belong to Ni-O stretching vibration [25]. Moreover, the steep stretching vibration peak of dissociative O-H at 3630cm^{-1} indicating the interlayer space of graphene is enlarged after the addition of $Ni(OH)_2$ sheet. So the residual O-H of reduced graphene oxide becomes more active. This confirms that the combination of $Ni(OH)_2$ and graphene enhances the single component's performance. The synergistic effect plays a vital role for the promotion of composites capacitive performance.

In order to obtain more information about graphene/$Ni(OH)_2$ composite, Raman spectroscopy (Fig.2C) has also been characterized. The characteristic peaks of first-order G-mode and disorder-induced D bands both appear for graphene and graphene/$Ni(OH)_2$ [26, 27]. A tiny shift from 1345 to 1352 cm^{-1} and from 1577 to 1594 cm^{-1} is observed. This is due to the introduction of nickel hydroxide to increase the disordered distribution of graphene, which increases the energy of graphene. Furthermore, the $Ni(OH)_2$ intercalation enhance the material structure integrity due to the decrease the collapses of graphene. In fact, the I_D/I_G ratio changed from 1.38 to 0.98, which is a measure of the defects in the carbon network. It indicate that graphene/$Ni(OH)_2$ gives full play to the properties of graphene.

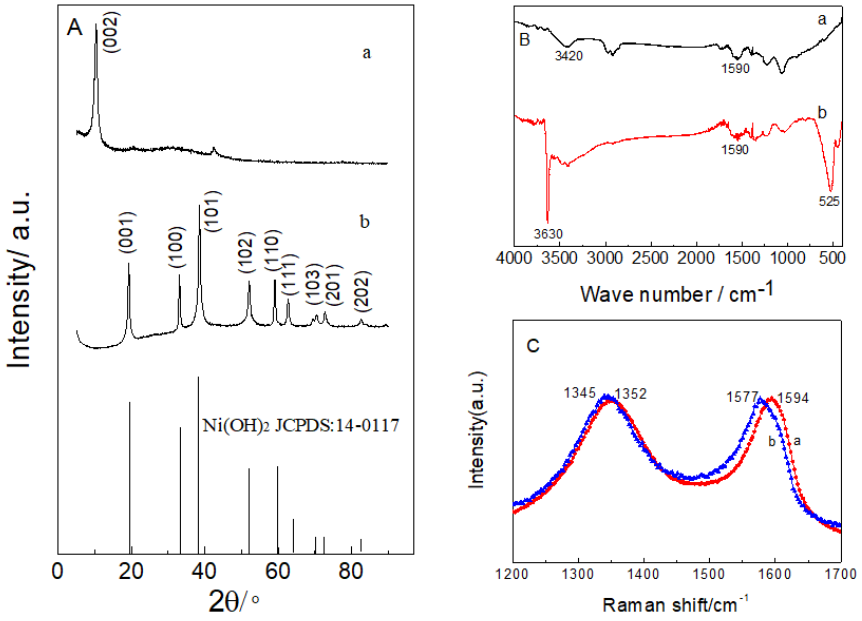

Figure 2. (A) XRD, (B) IR and (C) Raman spectra of graphene (a) and G3(b).

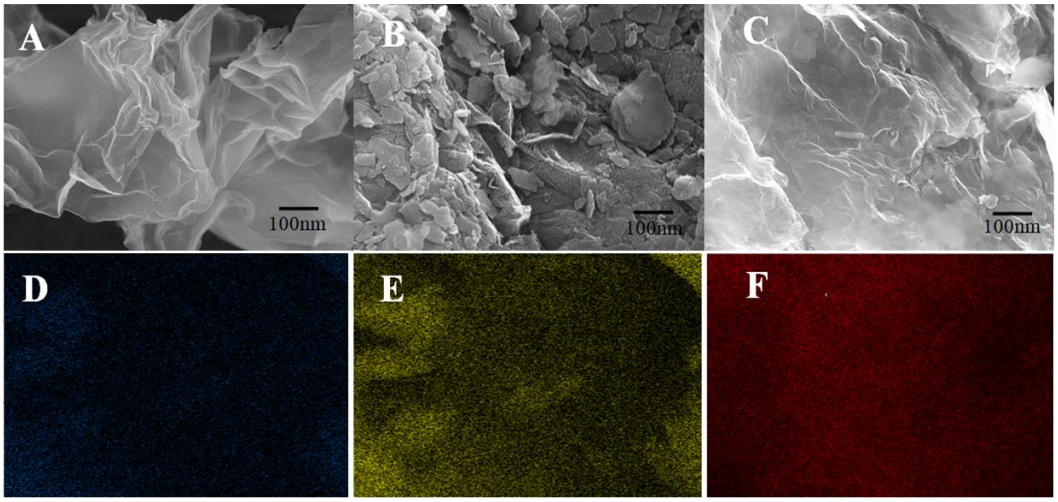

Figure 3. SEM images of graphene (A), $Ni(OH)_2$ (B), G3(C) and EDX element dispersion of C(D), O (E) and Ni (F) of G3.

SEM images of graphene, G3, $Ni(OH)_2$ and the EDX pattern of G3 are given in Fig. 3. It can be seen that graphene is a lamellar structure, which consist of several layers which as thin as a cicada's wings stacked on top of each other (Fig. 3A). $Ni(OH)_2$ is a sheet structure (Fig. 3B), a piece of irregular superposition together. graphene /$Ni(OH)_2$ sample (G3) is layered structure (Fig. 3C). The β-$Ni(OH)_2$ flake is uniformed distributed on the graphene surface. The EDX results further confirm the exist of $Ni(OH)_2$ and graphene in G3, and give a distinct view of homodisperse of $Ni(OH)_2$ and graphene.

To understand why the $Ni(OH)_2$ flake formed uniformed on graphene surface, a formation mechanism is summarized as follows: the addition of $Ni(C_2H_3O_2)_2$ solution provides numerous Ni^{2+}

nucleation centers on the graphene surface because where there are lots of negative charges carried by oxygen functional groups which could absorb Ni^{2+}. As the increasing of reaction temperature, Ni^{2+} is hydrolyzed to β-$Ni(OH)_2$ as well as the oxygen functional groups are reduced, so GO become graphene. As the anisotropy of β-$Ni(OH)_2$ crystals, the flake structure will be formed at certain direction. And graphene is also sheet structure and remains some oxygen functional groups on its surface. These oxygen functional groups form hydrogen bond with $Ni(OH)_2$, as a results, the $Ni(OH)_2$ flakes uniformed obtained on the graphene surface.

3.2 Electrochemistry performance

The electrochemical behavior of graphene/$Ni(OH)_2$ is evaluated by cyclic voltammograms and galvanostatic charge–discharge measurements. Fig. 4A shows the CV curves of graphene, G3, and $Ni(OH)_2$ measured at 50 mV s^{-1} in 6 mol L^{-1} KOH solution. The integral area of G3 is far larger than that of graphene and $Ni(OH)_2$. This mean the sandwich structure graphene /$Ni(OH)_2$ not is the simple mixture, it fully realizes the super performance of graphene and $Ni(OH)_2$ by synergistic effect. A pair of well-defined redox peaks corresponds to the equation (4) is exhibited for G3 [28]

$$\beta\text{-}Ni(OH)_2+OH^- \rightarrow \beta\text{-}NiOOH+H_2O+e^- \quad (4)$$

The oxidation peak at around 0.37 V and the reduction peak at about 0.1 V are strongly shifted compared with the single $Ni(OH)_2$ (0.29V and 0.13V). This means that the $Ni(OH)_2$ component of the as-prepared graphene /$Ni(OH)_2$ is more easily oxidized than that single $Ni(OH)_2$. It is owning to the insert of graphene enlarged the interlayer spacing of $Ni(OH)_2$ and more active sites are exposed, which is beneficial to the transfer of ion and proton.

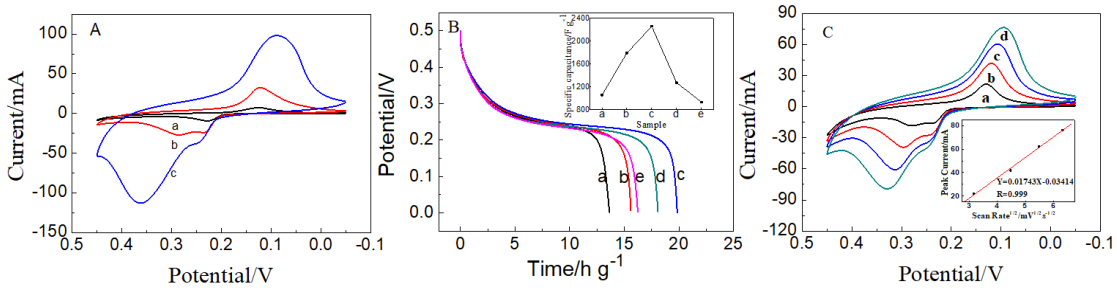

Figure 4. (A) CVs of graphene(a), $Ni(OH)_2$(b) and graphene/$Ni(OH)_2$ (G3) (c) at 50 mV s^{-1}in 6 M KOH, (B) Discharging curves of the G1 (a), G2 (b), G3(c), G4 (d), G5 (e) and inset is their specific capacitance. (C) The relationship of reduction peak current and square root of scan rate of G3

The discharge curves at 12.5 A g^{-1} of G1, G2, G3, G4, and G5 are given in Fig. 4B. There is a long discharge platform for every sample. At first with the increasing of Ni^{2+} concentration, the discharge time increases. When the ratio of C to Ni is equals to 1:7, the discharge time is the longest. And the supreme specific capacitance is 2256 F g^{-1}. Then the further increasing of Ni concentration causes the discharging time decreasing. This further confirms that the graphene /$Ni(OH)_2$ is not the simple mixture of two component, they do effect each other with synergistic effect. Due to the storage

energy mechanisms of graphene and $Ni(OH)_2$ are totally different. At certain ratio their synergistic effect works better than at the other conditions. The uniform layered structure not only enhances the utilization of the surface area of graphene, but also makes $Ni(OH)_2$ disperses well in graphene /$Ni(OH)_2$. Thus the nature of $Ni(OH)_2$ could also be fully exploited.

In order to excavate the dynamics feature of graphene /$Ni(OH)_2$ in the process of charging and discharging. The relationship of cyclic voltammogram reduction peaks current and square root of scan rate of G3 are expressed in Fig.4C. The linear correlation is found between the reduction peak current and the square rate of scan rate, and the coefficient of correlation (R) is equal to 0.998. This confirms that the electron transfer behave of G3 during electrochemical redox process are controlled by the rate of diffusion. It is coincide with the conclusion of Fig.4A that the oxidation reaction of $Ni(OH)_2$ to NiOOH is a fast step, and the parameters influence the diffusion of OH^- ion will determine the capacitance performance of materials. This sandwich structure graphene/$Ni(OH)_2$ made the $Ni(OH)_2$ well dispersed and so $Ni(OH)_2$ is more easy to be oxidized than packed $Ni(OH)_2$ sheets. As a results, this sandwich structure graphene/$Ni(OH)_2$ presents a wonderful capacitance performance, and it is superior to some reported similar materials, which detail data are exhibited in Table 1.

The cycle life is a vital parameter for supercapacitor. The cycle performance of G3 is displayed in Fig.5. At the first stage of 800 cycles, its specific capacitance remains 2256 F g^{-1} without any changes. Then, the slightly decrease appears and its value deceased 6 % after 7000 cycles and reaches 2125 F g^{-1}. The retention of 93 % shows the superior cycle stability of composite.

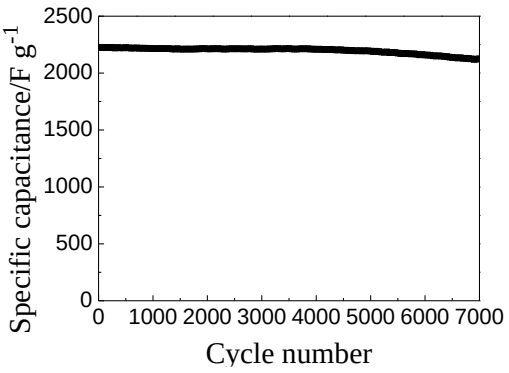

Figure 5. The specific capacitance of 7000 cycles

Table 1. Specific capacitance of relevant materials at different current density

electrode	electrolyte	Specific capacitance(F g^{-1})	Current density	Ref.
Graphene/$Ni(OH)_2$	6M KOH	2256	12.5A g^{-1}	This work
$Ni(OH)_2$/CNTs/graphene	6M KOH	2868.5	0.5 A g^{-1}	[29]
β-$Ni(OH)_2$@rGO	6M KOH	1710	2 A g^{-1}	[30]
Graphene/$Ni(OH)_2$	6M KOH	2053	0.3A g^{-1}	[31]
$Ni(OH)_2$/graphene/ CNTs	6M KOH	1170.38	0.2A g^{-1}	[32]
$Ni(OH)_2$/graphene	6M KOH	3408	1A g^{-1}	[33]
$LaCO_3OH$-$Ni(OH)_2$@RGO	6M KOH	572.47	50mVs^{-1}	[34]
G/GO/$Ni(OH)_2$	6M KOH	1510	2 A g^{-1}	[35]

4. CONCLUSIONS

In this paper the sandwich structure graphene /$Ni(OH)_2$ are obtained through convenient one-pot hydrothermal method without any additive treatment. It shows excellent capacitive performance in strong basic solution. The top specific capacitance is 2256 F g^{-1} at 12.5 A g^{-1} in 6M KOH solution. It is worth noting that 93% capacitance is retained after 7000 cycles. The extraordinary electrochemical performance is attributed to the sandwich structure of graphene /$Ni(OH)_2$, which maximally integrates the merits of both components. This confirms that sandwich structure graphene/$Ni(OH)_2$ is a promising capacitive materials in the case of energy application.

References

1. Q. Jiang, N. Kurra, M. Alhabeb, Y. Gogotsi and H.N. Alshareef, *Adv. Energy Mater*., 8 (2018) 10.
2. S. Yang, S.L. Wang, X. Liu and L. Li, *Carbon*, 147 (2019) 540.
3. A. Alameen, T.T. Jin, C.F. Xue, X.L. Ma, X. Du and X.G. Hao, *J. Solid State Electrochem*., (2020) DOI: 10.1007/s10008-020-04852-3.
4. D.Y. Tang, Y.Y. Luo, W.D. Lei, Q. Xiang, W. Ren, W.C. Song, K. Chen and J. Sun, *Appl. Surf. Sci*., 462 (2018) 862.
5. S.Q. Zhao, L.B. Dong, B. Sun, K. Yan, J.Q. Zhang, S.W. Wan, F.R. He, P. Munroe, P.H.L. Notten and G.X. Wang, *Small*, 16 (2020) 10.
6. K.X. Tang, T.Z.X. Hong, L.M. You and K. Zhou, *J. Mater. Chem*. A, 7 (2019) 26693.
7. X. Liang, Q.F. Wang, Y. Ma and D.H. Zhang, *Dalton Trans*., 47 (2018) 17146.
8. L.Q. Fan, F. Pan, Q.M. Tu, Y. Gu, J.L. Huang, Y.F. Huang and J.H. Wu, *Int. J. Hydrog. Energy*, 43 (2018) 23372.
9. W.J. Liang, S.L. Wang, Y.X. Zhang, J. Gu, K.D. Zhu, J. Zhong and X.R. Wang, *J. Alloys Comp*., 849 (2020) 11.
10. J. Orozco-Messana, R. Daly and I.F. Zanchetta-Chittka, *Ceram. Int.*, 46 (2020) 24831.
11. W. Wu, P. Xia, Y.W. Xuan, R. Yang, M. Chen and D.L. Jiang, *J. Nanotechnol*., 31 (2020) 9.
12. W. Ge, A. Encinas, M.F. Ruiz and S.X. Song, *Script. Mater*., 186 (2020) 79.
13. K.S. Novoselov, A.K. Geim, S.V. Morozov, D. Jiang, Y. Zhang, S.V. Dubonos, I.V. Grigorieva and A.A. Firsov, *Science*, 306 (2004) 666.
14. A. Hashimoto, K. Suenaga, A. Gloter, K. Urita and S. Iijima, Direct evidence for atomic defects in graphene layers, *Nature*, 430 (2004) 870.
15. S.M. Li, K. Yang, P. Ya, K.R. Ma, Z. Zhang and Q. Huang, *Appl. Surf. Sci*., 503 (2020) 9.
16. N. Xiang, J.G. Huang, H.G. Zhao, C.J. Liu and X.J. Liu, *Z. Phys. Chemie-Int. J. Res. Phys. Chem. Chem. Phys.*, 230 (2016) 1711.
17. Q.X. Zhou, W.W. Ju, Y.L. Yong, Q. Zhang, Y.L. Liu and J.L. Li, *Carbon*, 170 (2020) 368.
18. F. Dang, Z. Yang, P. Yang, Y. Su and Y. Liu, *J. Mater. Sci*., 56 (2021) 2506.
19. E. Redondo, L.W. Le Fevre, R. Fields, R. Todd, A.J. Forsyth and R.A.W. Dryfe, *Electrochim. Acta*, 360 (2020) 10.
20. D. Bhattacharjya, C.H. Kim, J.H. Kim, I.K. You, J.B. In and S.M. Lee, *Appl. Surf. Sci.*, 462 (2018) 353.
21. Y.W. Hong, J.L. Xu, J.S. Chung and W.M. Choi, *J. Mater. Sci. Technol*., 58 (2020) 73.
22. X.Y. Zhang, H.S. Wang, L.L. Shui, G.F. Zhou, X. Wang, R.G. Ma and J.C. Wang, *Sci. China Mater*., (2020) DOI: 10.1007/s40843-020-1427-0
23. Y.T. Zhou, M. Liu, H.Y. Yang, Q. Liu, W.D. Li and C.M. Yu, *Synth. Met*., 267 (2020) 13.
24. F. Ali, N. Agarwal, P.K. Nayak, R. Das and N. Periasamy, *Curr. Sci.*, 97 (2009) 682.
25. X.D. Liu, H. Masato, X.G. Zheng, D.D. Meng and Q.X. Guo, *Chin. Phys. Lett*., 28 (2011) 4.
26. V.I. Korepanov, E.N. Kabachkov, S.A. Baskakov and Y.M. Shul'ga, *Russ. J. Phys. Chem*. A, 94

(2020) 2250.
27. E.F. Sheka, Y.A. Golubev and N.A. Popova, *J. Nanomater*., 10 (2020) 22.
28. A. Pimsawat, A. Tangtrakarn, N. Pimsawat and S. Daengsakul, *Sci. Rep*., 9 (2019) 11.
29. T.T. Liu and M.T. Ji, *Ionics*, 25 (2019) 287.
30. N. Parveen, S.A. Ansari, S.G. Ansari, H. Fouad and M.H. Cho, *New J. Chem*., 41 (2017) 10467.
31. H. Chai, X. Peng, T. Liu, X.H. Su, D.Z. Jia and W.Y. Zhou, *RSC Adv*., 7 (2017) 36617.
32. Y.F. Liu, G.H. Yuan, Z.H. Jiang, Z.P. Yao and M. Yue, *J. Alloys Comp*., 618 (2015) 37.
33. M.M.M. Mohammed, A.G. Abd-Elrahim and D.M. Chun, *Mater. Chem. Phys*., 244 (2020) 122701.
34. T. Lv, Z.N. Xu, W. Hong, G.F. Li, Y.W. Li and L.S. Jia, *Chem. Eng. J.*, 382 (2020) 123021.
35. J. Tian, Q. Shan, X.L. Yin and W. Wu, *Adv. Powder Technol*., 30 (2019) 3118.